

Vortex excitations in binary mixture of trapped Bose-Einstein condensates

Dmitry V. Skryabin *

Department of Physics and Applied Physics, University of Strathclyde, Glasgow, G4 0NG, United Kingdom
(19 January, 2000)

Elementary excitations of vortices placed in one component of a binary mixture of Bose-Einstein condensates have been studied using perturbative and numerical solutions of the linearised equations for excitations and numerical simulation of the coupled Gross-Pitaevskii equations. Two distinct instabilities originating from resonances of the excitations have been found. One leads to the vortex *drift* out of the condensate. Second is the *splitting* of the higher order vortices into unit ones. Stabilizing role played by the vortex free component of the condensate has been revealed. Several distinct scenarios of the splitting resulting in different dynamics of the unit vortices have been described.

I. INTRODUCTION

Quantized vortex recently observed in a dilute ultracold gas of ^{87}Rb atoms [1] is one of the most spectacular evidences of the superfluid properties of atomic gases below transition temperature for formation of Bose-Einstein condensate (BEC). The vortex was created in one component of the binary mixture of the hyperfine states of ^{87}Rb following an ingenious suggestion by Williams and Holland [2] to rotate one component around the other in presence of a strong linear coupling of the condensates induced by the microwave field. Recent measurements of strong heating of the BEC pierced by a moving laser beam have also provided an indirect experimental evidence for formation of vortices in a single component condensate [3].

Properties of vortices in ultracold atomic gases have been subject of the intensive theoretical investigations over the last several years, see e.g. [4–10] [11–17]. Most of these studies have been focused on the scalar Gross-Pitaevskii (GP) equation describing superfluid component of ultracold gases. Characteristic frequencies of the elementary excitations of the unit vortices have been calculated numerically [8,14] and asymptotically in the Thomas-Fermi limit [9,10] and in the limit of weak interparticle interaction [9,12] in both stationary and rotating traps. It has been shown, solving linearised equations for excitations, that unit vortices in the singly component condensates (scalar GP equation) are dynamically stable, i.e. all characteristic frequencies are real, and that higher order vortices can be stable or unstable [15], depending from the system parameters.

An important feature of the experimental setup used in [1] is that vortex is created in one of two components of the condensate mixture, while the second component is vortex free. When external driving is switched off evolution of the wave functions of both condensates obey coupled GP equations. Studies of the vortex free two-species

condensates have been reported in the large number of papers, see [21,22] and references therein. Vortex dynamics in the coupled GP equations was previously studied numerically in Ref. [23], where regime of the periodic transfer of the unit vortex between two condensates has been reported. Recent papers [24,25] also reported existence of the vortices in more complex three component condensates.

Calculations of the spectrum of the second variation of the Hamiltonian [23] show that unit vortex placed in one of the component of the double condensate is not a local minimum of the Hamiltonian. Therefore dissipation, due to presence of the normal fluid, i.e. particles out of the condensate, will drive condensate into energetically favourable vortex free ground state, similar to what has been found in the single-species condensates [6,18–20]. Thus vortex free component does not stabilise vortex against dissipative effects.

Spectral properties of the elementary excitations of the unit and higher-order vortices in double condensates described by the linearisation of the coupled GP equations have remained practically unknown. Knowledge of these properties holds a key to understanding of the origin of the dynamical instabilities and mechanisms of their suppression and study of these problems is the primary objective of this work.

In the next section we introduce coupled GP equations and describe their general properties. Then, in section III, we derive linearised system describing spectrum of the vortex excitations and present several exact solutions. In section IV we develop perturbative theory to find characteristic frequencies of the excitations of the unit vortices in the weakly interacting condensates. Remarkably, this theory gives an approximate criterion predicting possible instabilities of the vortex. In the following sections we proceed with detail numerical study of the linearised system for the elementary excitations supported by the simulation of the vortex dynamics.

*URL: [www://http.cnqo.strath.ac.uk/~dmitry](http://http.cnqo.strath.ac.uk/~dmitry)

II. GROSS-PITAEVSKII EQUATIONS

Wave functions $\psi_{1,2}$ of two-species condensate inside an axial harmonic trap at zero temperature obey coupled GP equations [21]

$$\begin{aligned} i\hbar\partial_t\psi_1 &= -\frac{\hbar^2}{2m}\vec{\nabla}^2\psi_1 + \frac{1}{2}m\omega^2(r^2 + \sigma^2z^2) \\ &+ (u_{11}|\psi_1|^2 + u_{12}|\psi_2|^2)\psi_1, \\ i\hbar\partial_t\psi_2 &= -\frac{\hbar^2}{2m}\vec{\nabla}^2\psi_2 + \frac{1}{2}m\omega^2(r^2 + \sigma^2z^2) \\ &+ (u_{22}|\psi_2|^2 + u_{21}|\psi_1|^2)\psi_2, \end{aligned} \quad (1)$$

where for simplicity we have neglected by possible differences of atomic masses $m_{1,2} = m$ and trap frequencies, $\omega_{1,2} = \omega$, $\sigma_{1,2} = \sigma$. Coefficients $u_{ij} = 4\pi\hbar^2 a_{ij}/m$ characterise intra- and inter-species interaction with corresponding scattering lengths $a_{11} \neq a_{22}$ and $a_{12} = a_{21}$.

At this point we introduce dimensionless time and space variables $\tilde{t} = \omega t$ and $\tilde{r}, \tilde{z} = r, z/a_{ho}$ and normalisation for the wave functions $\tilde{\psi}_{1,2} = a_{ho}^3 \psi_{1,2}/\sqrt{N_{1,2}}$, where $a_{ho} = \sqrt{\hbar/(m\omega)}$ is the harmonic oscillator strength and $N_{1,2} = \int dV |\psi_{1,2}|^2$ are the number of particles. We will consider the quasi-2D model to simplify our numerical study. This approximation was previously used in several works, see e.g. [15,23], and it is applicable not only for pancake traps, $\sigma \gg 1$, but also captures main qualitative features of spherical traps. To make further reduction of Eqs. (1) we redefine the wave functions once more:

$$\tilde{\psi}_{1,2} = \left[\frac{\sigma}{2\pi}\right]^{1/4} \Psi_{1,2}(\tilde{r}, \theta, \tilde{t}) e^{-\sigma\tilde{z}^2/4} e^{-i\mu_{1,2}\tilde{t} - i\sigma\tilde{t}/2}, \quad (2)$$

where $\mu_{1,2}$ are the chemical potentials. Dropping tilde we find that $\Psi_{1,2}$ obey

$$\begin{aligned} i\partial_t\Psi_1 &= \left[\hat{T} + \hat{V} - \mu_1 + g(\beta_{11}|\Psi_1|^2 + \beta_{12}|\Psi_2|^2)\right] \Psi_1, \\ i\partial_t\Psi_2 &= \left[\hat{T} + \hat{V} - \mu_2 + g(\beta_{22}|\Psi_2|^2 + \beta_{12}|\Psi_1|^2)\right] \Psi_2, \end{aligned} \quad (3)$$

where \hat{T} is the kinetic energy operator, $\hat{V} = r^2/4$ is the potential energy of the harmonic trapping, $g = 8\sqrt{\pi\sigma}N_1a_{11}/a_{ho}$, $\beta_{12} = a_{12}/a_{11}$, and $\beta_{22} = a_{22}/a_{11}$. $\beta_{11} = 1$ and it is left in the equations for the sake of symmetry.

Eqs. (3) can also be presented in the Hamiltonian form

$$i\partial_t\Psi_j = \frac{\delta H}{\delta\Psi_j^*}, \quad j = 1, 2. \quad (4)$$

$H = \int r dr d\theta (\mathcal{E} - \mu_1|\Psi_1|^2 - \mu_2|\Psi_2|^2)$ is the Hamiltonian functional and \mathcal{E} is the energy density:

$$\begin{aligned} \mathcal{E} &= |\vec{\nabla}\Psi_1|^2 + |\vec{\nabla}\Psi_2|^2 + (|\Psi_1|^2 + |\Psi_2|^2)/(4r^2) \\ &+ g[\beta_{11}|\Psi_1|^4 + \beta_{22}|\Psi_2|^4 + 2\beta_{12}|\Psi_1|^2|\Psi_2|^2]/2. \end{aligned} \quad (5)$$

Invariances of H with respect to the infinitesimal rotations $\theta \rightarrow \theta + \delta\theta$ and two parameter phase transformation

$$(\Psi_1, \Psi_2) \rightarrow (\Psi_1 e^{i\phi_1}, \Psi_2 e^{i\phi_2}), \quad (6)$$

result in conservation of the total angular momentum and of the number of particles in each component.

$\mu_{1,2}$ are fixed by the normalization conditions

$$\int r dr d\theta |\Psi_1|^2 = 1, \quad \int r dr d\theta |\Psi_2|^2 = \frac{N_2}{N_1} \equiv n. \quad (7)$$

Radially symmetric stationary solutions can be presented in the form $\Psi_j = A_j(r)e^{il_j\theta}$. We will focus our attention on the stationary states with vortex in one of the components. Using the method described in [1,2] only such vortices can be practically created. For concreteness we will fix $l_1 = 0$ and $l_2 \neq 0$. Transverse profiles of the vortex solutions $A_j(r)$ were found numerically using Newton method applied to Eqs. (3) with $\partial_t = 0$ and subject to the boundary conditions $A_{1,2}(r \rightarrow 0) \rightarrow r^{l_{1,2}}c_{1,2}$ and $A_{1,2}(r \rightarrow \infty) \rightarrow 0$, where $c_{1,2}$ are real constants.

Harmonic potential \hat{V} and terms proportional $|\Psi_1|^2$ can be neglected if $n \gg 1$ and r is not too large. In this approximation vortex free component of the condensate can be qualitatively considered as an eigenstate of the linear Schrödinger equation with potential created by the vortex. More details on this issue can be found in [26], where variety of stationary solutions of the coupled GP equations without harmonic potential were considered in the context of nonlinear optics.

III. LINEARISED EQUATIONS FOR EXCITATIONS

To study vortex dynamics in presence of perturbations we linearise Eqs. (3) plus a pair of complex conjugated equation using substitutions

$$\begin{aligned} \Psi_j &= (A_j(r) + \epsilon_j^-(r, \theta, t))e^{il_j\theta}, \\ \Psi_j^* &= (A_j(r) + \epsilon_j^+(r, \theta, t))e^{-il_j\theta}, \end{aligned} \quad (8)$$

where ϵ_j^\pm are small excitations. Resulting linear eigenvalue problem is

$$i\partial_t\vec{\epsilon} + \hat{L}\vec{\epsilon} = 0, \quad (9)$$

where $\vec{\epsilon} = (\epsilon_1^-, \epsilon_1^+, \epsilon_2^-, \epsilon_2^+)^T$ and operator \hat{L} is

$$\begin{bmatrix} -\hat{L}_1^+ & -g\beta_{11}A_1^2 & -g\beta_{12}A_1A_2 & -g\beta_{12}A_1A_2 \\ g\beta_{11}A_1^2 & \hat{L}_1^- & g\beta_{12}A_1A_2 & g\beta_{12}A_1A_2 \\ -g\beta_{12}A_1A_2 & -g\beta_{12}A_1A_2 & -\hat{L}_2^+ & -g\beta_{22}A_2^2 \\ g\beta_{12}A_1A_2 & g\beta_{12}A_1A_2 & g\beta_{22}A_2^2 & \hat{L}_2^- \end{bmatrix},$$

$$\begin{aligned}
\hat{L}_1^\pm &= -\frac{1}{r} \frac{\partial}{\partial r} r \frac{\partial}{\partial r} - \frac{1}{r^2} \left(\frac{\partial}{\partial \theta} \pm i l_1 \right)^2 \\
&+ \hat{V} - \mu_1 + 2g\beta_{11}A_1^2 + g\beta_{12}A_2^2, \\
\hat{L}_2^\pm &= -\frac{1}{r} \frac{\partial}{\partial r} r \frac{\partial}{\partial r} - \frac{1}{r^2} \left(\frac{\partial}{\partial \theta} \pm i l_2 \right)^2 \\
&+ \hat{V} - \mu_2 + 2g\beta_{22}A_2^2 + g\beta_{12}A_1^2.
\end{aligned}$$

\hat{L} is a non-self-adjoint operator and therefore it can have complex eigenvalues. Presence of an eigenvalue with negative imaginary part implies *dynamical* instability of a stationary state under consideration, if such eigenvalues are absent then the state is *dynamically* stable. In the latter case excitations of this state with small absolute values of eigenvalues represent some practical interest, because these excitations are relatively well localised and thus they are easily excited and have long life-time. Note, that choice of the normalisation of the eigenmodes of \hat{L} is irrelevant for the problems considered below.

Thus our primary interest is understanding of the spectral properties of the eigenvalue problem

$$\hat{L}\vec{\xi} = \lambda\vec{\xi}. \quad (10)$$

Infinitesimal variations of ϕ_j generate two doubly degenerate zero-eigenvalues of \hat{L} with eigenmodes $(A_1, -A_1, 0, 0)^T$ and $(0, 0, A_2, -A_2)^T$. Zero eigenvalue modes, however, are not very interesting because their excitations do not lead to the experimentally detectable breathing of the condensate, see e.g. [27]. Dipole modes are more practical in this sense. In the free condensate limit, $\hat{V} = 0$, Eqs. (3) are translationally invariant and therefore \hat{L} has two zero eigenvalues generated by infinitesimal translations. Galilean invariance is also restored in this limit and it is responsible for the fact that each of the zero eigenvalues is a doubly degenerate one. Harmonic trapping breaks translational and Galilean symmetries and modifies spectrum in such a way that \hat{L} acquires doubly degenerate $\lambda = \pm 1$ eigenvalues with eigenfunctions

$$\vec{\xi}_d^{(\pm)} = e^{\pm i\theta} \begin{bmatrix} \lambda \left(\frac{dA_1}{dr} \mp \frac{1}{r} l_1 A_1 \right) + \frac{1}{2} r A_1 \\ \lambda \left(\frac{dA_1}{dr} \pm \frac{1}{r} l_1 A_1 \right) - \frac{1}{2} r A_1 \\ \lambda \left(\frac{dA_2}{dr} \mp \frac{1}{r} l_2 A_2 \right) + \frac{1}{2} r A_2 \\ \lambda \left(\frac{dA_2}{dr} \pm \frac{1}{r} l_2 A_2 \right) - \frac{1}{2} r A_2 \end{bmatrix}, \quad (11)$$

where λ can take values ± 1 for both vectors. Eqs. (11) generalise expressions for the dipole modes previously derived for single-species condensates [10].

Our original equations are Hamiltonian ones therefore

$$Tr \hat{L} = 0, \quad (12)$$

and spectrum of \hat{L} is symmetric with respect to the both imaginary and real axis in the complex plane ($Re\lambda, Im\lambda$) [29].

IV. LOW-FREQUENCY EXCITATIONS OF UNIT VORTICES IN THE WEAKLY INTERACTING CONDENSATE

We begin our analysis considering weakly interacting condensate implying $g \ll 1$, $n \sim 1$. In this limit potential energy due to harmonic trapping \hat{V} strongly dominates over the interaction energy. In the context of vortices in single-species condensates this limit was recently considered in [12] and it is useful mainly because it allows to understand degeneracy of the spectrum at $g = 0$ and as a consequence origin of the elementary excitations and, possibly, of the dynamical instabilities. In this Section we will concentrate on the case of the unit vortex, i.e. $l_1 = 0$, $l_2 = 1$. Perturbation theory will be developed only up to the first order and then we will proceed with detail numerical analysis. Although second order theory is a straightforward exercise it is rather cumbersome in the two component case and can be subject of a separate investigation.

We substitute asymptotic expansions $\mu_{1,2} = \mu_{1,2}^{(0)} + g\mu_{1,2}^{(1)} + O(g^2)$, $A_{1,2} = A_{1,2}^{(0)} + gA_{1,2}^{(1)} + O(g^2)$ into the stationary version of Eqs. (3) and derive recurrent system of linear equations. In the zero approximation we have two uncoupled harmonic oscillator problems with eigenmodes

$$A_1^{(0)} = \frac{1}{\sqrt{2\pi}} e^{-r^2/4}, \quad A_2^{(0)} = \sqrt{\frac{n}{2\pi}} \frac{r}{\sqrt{2}} e^{-r^2/4}.$$

Using solvability condition of the first order problem we find asymptotic expressions for chemical potentials: $\mu_1 = 1 + g(2\beta_{11} + n\beta_{12})/(8\pi) + O(g^2)$, $\mu_2 = 2 + g(n\beta_{22} + \beta_{12})/(8\pi) + O(g^2)$.

Then we expand operator \hat{L} , its eigenvectors and eigenvalues into the series $\hat{L} = \hat{L}^{(0)} + g\hat{L}^{(1)} + O(g^2)$, $\vec{\xi} = \vec{\xi}^{(0)} + g\vec{\xi}^{(1)} + O(g^2)$, $\lambda = \lambda^{(0)} + g\lambda^{(1)} + O(g^2)$. Our primary interest is low lying excitations and therefore we restrict ourselves by the expansions near eigenvalues $\lambda^{(0)} = 0$ and $\lambda^{(0)} = 1$. Spectrum near $\lambda^{(0)} = -1$ is just the mirror image of the spectrum near $\lambda^{(0)} = 1$, see Eq. (12).

$\hat{L}^{(0)}$ has six zero eigenvalues with eigenvectors

$$\begin{aligned}
\vec{\xi}_{1,2}^{(0)} &= \frac{\vec{x}_{1,2}}{\sqrt{2\pi}} e^{-r^2/4}, \quad \vec{\xi}_{3,4}^{(0)} = \frac{r\vec{x}_{3,4}}{2\sqrt{\pi}} e^{-r^2/4}, \\
\vec{\xi}_5^{(0)} &= \frac{r\vec{x}_3}{2\sqrt{\pi}} e^{-r^2/4-2i\theta}, \quad \vec{\xi}_6^{(0)} = \frac{r\vec{x}_4}{2\sqrt{\pi}} e^{-r^2/4+2i\theta},
\end{aligned} \quad (13)$$

where $\vec{x}_j = (\delta_{1j}, \delta_{2j}, \delta_{3j}, \delta_{4j})^T$ and δ_{ij} is the Kroneker symbol.

Four eigenvalues corresponding to the eigenvectors $\vec{\xi}_{1,2,3,4}$ remain zero ones for any values of g , hence they

correspond to the neutral modes generated by the phase symmetries 6. Eigenvalues corresponding to $\vec{\xi}_{5,6}$ are $\lambda = \mp gn\beta_{22}/(8\pi) + O(g^2)$ and they produce low frequency branches in the excitation spectrum.

$\hat{L}^{(0)}$ has also six $\lambda^{(0)} = 1$ eigenvalues with eigenvectors

$$\begin{aligned}\vec{\xi}_7^{(0)} &= \frac{r\vec{x}_2}{2\sqrt{\pi}}e^{-r^2/4+i\theta}, \quad \vec{\xi}_8^{(0)} = \frac{r\vec{x}_2}{2\sqrt{\pi}}e^{-r^2/4-i\theta}, \\ \vec{\xi}_9^{(0)} &= \frac{\vec{x}_3}{\sqrt{2\pi}}e^{-r^2/4-i\theta}, \quad \vec{\xi}_{10}^{(0)} = \frac{(r^2/2-1)\vec{x}_4}{\sqrt{2\pi}}e^{-r^2/4+i\theta}, \\ \vec{\xi}_{11}^{(0)} &= \frac{r^2\vec{x}_4}{4\sqrt{\pi}}e^{-r^2/4+3i\theta}, \quad \vec{\xi}_{12}^{(0)} = \frac{r^2\vec{x}_4}{4\sqrt{\pi}}e^{-r^2/4-i\theta}.\end{aligned}\quad (14)$$

Considering excitations $\sim e^{-i\theta}$ we find one eigenvalue corresponding to the dipole mode $\vec{\xi}_d^{(-)}$ and another pair of eigenvalues is

$$\begin{aligned}\lambda &= 1 + \frac{g}{32\pi} \left(-3\beta_{12} - n\beta_{22} \right. \\ &\quad \left. \pm \sqrt{(3\beta_{12} + n\beta_{22})^2 - 8n\beta_{12}^2} \right) + O(g^2).\end{aligned}\quad (15)$$

Excitations $\sim e^{i\theta}$ are responsible for another dipole mode $\vec{\xi}_d^{(+)}$ and for a mode with eigenvalue deviating from zero only in the second order, i.e. $\lambda = 1 + O(g^2)$. Finally, an eigenvalue corresponding to $\vec{\xi}_{11}$ is $\lambda = 1 + g(n\beta_{22} - \beta_{12})/(16\pi) + O(g^2)$. Note, that excitations with an azimuthal quantum number J , i.e. proportional to $e^{iJ\theta}$, carry angular momentum J taken relatively of the angular momentum of the wave function itself.

Thus, there exist four positive and four negative characteristic frequencies with values close, but not equal, to ± 1 . It is important to emphasize that in a singly component condensate there are only 2 positive and 2 negative such frequencies. In our case excitations with angular momenta $+1$ and -1 have, among others, eigenvectors $\vec{\xi}_{7,8}$, which are linked with the vortex free part of the condensate. This results in extra splitting in the spectrum, see Eq. (15), and provides a channel for transfer of the angular momentum into the vortex free condensate component.

For β_{12} and β_{22} positive, the eigenvalues (15) become complex if

$$\frac{\beta_{22}}{\beta_{12}} < \frac{1}{n}(2\sqrt{2n} - 3).\quad (16)$$

The latter condition indicates onset of the vortex instability. Appearance of a pair of complex eigenvalues implies that their real parts become equal, i.e. the instability can be interpreted as due to *resonance* between two elementary excitations. Note, that even if condition (16) can not be satisfied for any realistic values of the parameters, then the same type of instability still can be expected, but out of the validity range of the perturbative expansion, see next Section for more details. Eq. (16) correctly captures tendency, which will be supported numerically

in the following Sections, that unit vortices are more stable if intraspecies interaction of atoms in the vortex containing part of the condensate is somewhat larger than interspecies interaction. Note, also that if first order corrections to eigenvalues (15) are real and nonzero, then second order theory can not capture possible appearance of complex eigenvalues for larger g .

V. NUMERICAL METHOD

Now we introduce numerical method used in the next sections to study spectral properties of \hat{L} . We consider only solutions of GP equations, which are θ periodic with period 2π . Therefore, $\vec{\xi}$ can be expressed as a superposition of its azimuthal harmonics $e^{iJ\theta}$ ($J = 0, \pm 1, \pm 2, \dots$) with coefficients depending on r and elementary excitations with different J can be considered as independent ones. This replaces study of the spectrum of the partial differential operator \hat{L} by study of the spectra of a set of the ordinary differential operator \hat{L}_J , where \hat{L}_J is simply \hat{L} with $(\partial_\theta \pm il_{1,2})^2$ replaced by $-(J \pm l_{1,2})^2$. This transformation greatly reduces computer time, because in the cases considered below only excitations with small J play an important role in the dynamics.

Set of the eigenvalue problems

$$\hat{L}_J \vec{\xi} = \lambda \vec{\xi}\quad (17)$$

was solved using second order finite differences. All four components of $\vec{\xi} = (\xi_1, \xi_2, \xi_3, \xi_4)^T$ obey zero boundary conditions at $r = \infty$. However, each component generally has its own boundary condition when $r \rightarrow 0$:

$$\begin{aligned}\xi_1 &\rightarrow r^{|J+l_1|}a_1, \quad \xi_2 \rightarrow r^{|J-l_1|}a_2, \\ \xi_3 &\rightarrow r^{|J+l_2|}a_3, \quad \xi_4 \rightarrow r^{|J-l_2|}a_4,\end{aligned}\quad (18)$$

where a_j are some constants. Spectrum of \hat{L}_0 preserves symmetry properties of the spectrum of \hat{L} . For any other J the symmetry with respect to the line $Re\lambda = 0$ is lost and property (12) is replaced by $Tr(\hat{L}_J + \hat{L}_{-J}) = 0$. Hence spectrum of \hat{L}_{-J} can be obtained as a mirror image of \hat{L}_J with respect to the line $Re\lambda = 0$.

VI. DRIFT OF UNIT VORTICES

To reduce number of the bifurcation parameters, we primarily focus on two choices of scattering lengths corresponding to the experimental values taken from [21]: $\beta_{22} = 1.03/0.97$, $\beta_{12} = 1/0.97$ ($\beta_{22} > \beta_{11}$) and $\beta_{22} = 0.97/1.03$, $\beta_{12} = 1/1.03$ ($\beta_{22} < \beta_{11}$). The former case corresponds to the vortex in the spin state $\langle F = 1, m_f = -1 \rangle$ of ^{87}Rb and the latter to the vortex in the state $\langle 2, 2 \rangle$. These two states will be called - state 1 and state 2.

In Ref. [23] authors reported that for $n = 1$ vortex in the state 1 is dynamically stable and in the state 2

is unstable. This result was verified by direct numerical simulation of GP equations without an explicitly shown analysis of the eigenvalues of the operator \hat{L} [23]. Below we will reveal bifurcation scenarios leading to the dynamical instability of the vortex and will study influence of the parameters g , n and β_{ij} on this instability. Note that n can be experimentally controlled by adjusting the frequency of the driving microwave field [1,21].

Theory developed in Section III suggests that perturbations with angular momenta ± 1 should play an important role in the dynamical stability of the unit vortices. No resonances of eigenfrequencies and hence no associated instabilities have been found, when vortex is in the state 1. In particular, eigenfrequencies described by Eq. (15) were found to separate with increasing of g , see Fig. 1. The situation is quite opposite when vortex is placed in the state 2. Figs. 2,3,4 show resonances of eigenfrequencies (15) and appearance of the corresponding instabilities. Although for $n = 1$ onset of the instability happens for $g < 1$, see Fig. 2(a), it can not be captured by the previously described asymptotic theory. It is clear from comparison of numerical and asymptotic results presented in Fig. 2(a), that Eq. (15) gives reasonable approximation only for $g < 0.05$.

The unstable modes of the vortex in the state 2 are of the dipole type therefore they growth leads to the initial displacement of the vortex from the trap center. Then at the nonlinear stage of the instability development vortex starts its drift to the condensate periphery on the curved background. This phenomenon is similar to the drift of an optical vortex displaced from the center of a gaussian beam [28]. The vortex on a low background carries less of the total angular momentum, compare to the momentum of the vortex positioned at the trap center. Lack of the angular momentum is compensated by two factors. First, vortex acquires a nonzero tangential velocity and therefore its trajectory is actually a spiral. Second, angular momentum, and vortex itself, become gradually transferred into the second condensate component, as it was numerically verified in [23].

In the limits $n \gg 1$ and $n \ll 1$ our model can be approximately considered as a single component condensate with ($n \gg 1$) or without ($n \ll 1$) vortex. Unit vortex and ground state of the single component condensate are known to be dynamically stable. Therefore drift instability disappears in both limits, see Fig. 5. Increase of g for fixed n also results in the suppression of the instability, see Figs. 2,3,4, which means that not only relative, but also absolute increase of the number of atoms in the vortex free component stabilizes the condensate.

Stability of the vortex in the state 1 indicate that relative value of the intra- and inter-species interaction plays an important role in the vortex dynamics. Dependencies of the growth rate of the drift instability vs strength of the inter-species interaction β_{12} are shown in Fig. 6. It is clear that strong interaction enhances the drift in-

stability and weak-interaction suppresses it. In the limit $\beta_{12} \ll 1$ vortex properties are similar to ones in the single component condensates.

If drift instability is absent, then dissipative effects still can result in the vortex drift. This phenomenon was predicted in the single component condensates by several authors [6,20]. Dissipation drives condensate into the global minimum of H , which is the vortex free state, along the path determined by the dipole like eigenmode. Excess of the angular momentum is simply dissipated during the vortex drift. Presence of the second condensate opens a channel for the angular momentum transfer from the vortex into the vortex free component. Thus drift instability can be interpreted as due to dissipation of the energy and momentum by the vortex free condensate component.

VII. DRIFT AND SPLITTING OF HIGHER ORDER VORTICES

Considering higher order vortices one can expect to find instability scenario which is qualitatively different from the drift instability of the unit vortices. This scenario is splitting into a set of unit vortices associated with $|J| > 1$ excitations. However, as we will see below the drift instability itself, $|J| = 1$, is also presented. It leads to displacement of the whole vortex from the trap center without splitting, at least at the onset of the instability.

Drift and splitting instabilities of the higher-order vortices appear as a result of resonances of the elementary excitations, similar to the case of unit vortices. Limit $n \ll 1$ corresponds to the vortex free condensate and therefore both instabilities are suppressed in these limits. In the limit $n \gg 1$ only drift instability is suppressed and one can recover periodic in n unstable bands of the splitting instabilities similar to the results reported for higher order vortices in a singly component condensate [15]. This should be contrasted with limit $g \gg 1$, where all the instabilities become suppressed. Note, that splitting itself was not explicitly analysed in [15]. It is also interesting to note that higher-order vortices in the free, $\hat{V} = 0$, single component condensate are dynamically stable [30]. Thus splitting can be considered as induced by the trapping. The vortex free condensate component plays crucial role in the drift instability, but will the latter one be presented without trapping or not remains an open problem. The higher order vortices are of course always structurally unstable and can be splitted applying even tiny perturbations breaking cylindrical symmetry.

A. Double vortices

Considering double vortex we have found that it can be unstable with respect to the $|J| = 1, 2$ excitations. Double vortex in the state 1 has been found surprisingly

stable. One has to take relatively small values of g and large n to find splitting instability, see Fig. 7. Vortex in the state 2 is more unstable in a sense that splitting exists already for $n \sim 1$, see Fig. 8. As it is evident from Fig. 8 either drift or splitting instability can dominate vortex dynamics. If drift instability is dominant, then vortex first gets displaced from the trap center and only then splits into the unit ones, see Fig. 9. The latter happens due to the curved background which breaks cylindrical symmetry with respect to the vortex axis. After the splitting vortices remain close to each other and move towards the condensate periphery.

The dynamics is quite different when splitting instability is dominant, see Fig. 10. In this case unit vortices appear straight at the onset of the instability development and spiral out of the condensate center being always positioned symmetrically with respect to the trap center. After a certain period of time vortices move back to the trap center and condensate state close to the initial one is restored, see Fig. 10, then the cycle is repeated with gradually worsening degree of periodicity.

Angular momentum and vorticity become partially transferred into the second condensate as a result of the growth of the unstable modes in both cases. Dynamical evolution of the transverse profiles of the phases, see Fig. 11, corresponding to the density profiles shown in Fig. 10, explicitly shows that black spots appearing in the second condensate are indeed unit vortices. Examples of the phase profiles of the ideal unit and double vortices are shown in Fig. 12 to ease understanding of the Fig. 11.

Dependencies of the growth rates of the drift and splitting instabilities of the double vortex vs strength of the inter-species interaction β_{12} are shown in Fig. 13. Drift instability starts to dominate over the splitting with increasing of β_{12} , which is another verification of the fact that vortex drift is induced by the nonlinear coupling with vortex free component. For small values of β_{12} only splitting instability is presented. Position of the left most band of the splitting instability depends on the choice of n and g and for certain values of these parameters splitting can also be presented for $\beta_{12} = 0$, see [15].

B. Triple vortices

Triple vortex has been found unstable with respect to the perturbations with $|J| = 1, 2, 3$. Instabilities of the vortex in the state 1 are suppressed in the limits $n \ll 1$ and $g \gg 1$, see Fig. 14. Compare to the double vortex this suppression happens for smaller n and larger g , which means that on overall triple vortex is a less stable structure. Instability growth rates of the vortex in the state 2 vs n are shown in Fig. 15. One can see that $|J| = 2$ instability dominates in most of the cases. All

components of the corresponding eigenmode have zero boundary conditions at the trap center, see Eqs. (18). Therefore one can expect that growth of this mode will develop into a spatial structure preserving vortex at the trap center. Indeed, numerical simulation shows that two unit vortices split radially from the vortex core leaving the third one resting at the center, see Fig. 16.

Small gaussian like perturbations of the vortex core match spatial profiles of the $|J| = 3$ eigenmodes much better than of the $|J| = 2$ ones, see Eqs. (18). Providing that such perturbation are applied to the initial state, the $|J| = 3$ instability can win competition with $|J| = 2$ one, even if the ratio of the spontaneous growth rates favours the $|J| = 2$. Growth of the $|J| = 3$ instability leads to the breaking of the triple vortex into a triangular structure of the unit vortices moving away from the trap center, see Fig. 17.

VIII. SUMMARY

Low lying eigenfrequencies, including ones generating instability of the unit vortex placed in one component of a binary mixture of BEC, have been calculated applying perturbative theory in the limit of the weak interparticle interaction. Results of the perturbative theory have been verified and significantly extended using numerical analysis of the linearised equations for excitations and direct numerical simulation of the coupled Gross-Pitaevskii equations. Two main instability mechanisms have been identified and their dependencies on the relative number of the particles in the condensates and on the strength of the inter-species interaction have been studied. First mechanism is the *drift* instability induced by the vortex free component of the condensate and resulting in the motion of the vortex out of the condensate center to its periphery. Second mechanism is the *splitting* of the higher order vortices into unit ones. Absolute and/or relative increase of the number of particles in the vortex free condensate component has been found to have stabilizing effect.

ACKNOWLEDGMENTS

Author acknowledges discussions with S.M. Barnett and W.J. Firth. Numerical part of the work was significantly speeded up due to access to the computer equipment obtained via U.K. EPSRC grant GR/M31880 and assistance of G. Harkness and R. Martin.

-
- [1] M.R. Matthews, B.P. Anderson, P.C. Hajan, D.S. Hall, C.E. Wieman, and E.A. Cornell, Phys. Rev. Lett. **83**, 2498 (1999).
- [2] J.E. Williams and M.J. Holland, Nature **401**, 568 (1999).
- [3] C. Raman, M. Köhl, R. Onofrio, D. S. Durfee, C. E. Kulewicz, Z. Hadzibabic, and W. Ketterle, Phys. Rev. Lett. **83**, 2502 (1999).
- [4] M. Edwards, R.J. Dodd, C.W. Clark, P.A. Ruprecht, and K. Burnett, Phys. Rev. A **53**, R1950 (1996).
- [5] F. Dalfovo and S. Stringari, Phys. Rev. A **53**, 2477 (1996).
- [6] D.S. Rokhsar, Phys. Rev. Lett. **79**, 2164 (1997).
- [7] S. Sinha, Phys. Rev. A **55**, 4325 (1997).
- [8] R.J. Dodd, K. Burnett, M. Edwards, and C.W. Clark, Phys. Rev. A **56**, 587 (1997).
- [9] F. Zambelli and S. Stringari, Phys. Rev. Lett. **81**, 1754 (1998).
- [10] A.A. Svidzinsky and A.L. Fetter, Phys. Rev. A **58**, 3168 (1998).
- [11] E. Lundth, C.J. Pethick, and H. Smith, Phys. Rev. A **58**, 4816 (1998).
- [12] M. Linn and A.L. Fetter, Phys. Rev. A **60**, 4886 (1999).
- [13] D.F. Feder, C.W. Clark, and B. Schneider, Phys. Rev. Lett. **82**, 4956 (1999).
- [14] J.J. Garcia-Ripoll and V.M. Pérez-Garcia, Phys. Rev. A **60**, 4864 (1999).
- [15] H. Pu, C.K. Law, J.H. Eberly, and N.P. Bigelow, Phys. Rev. A **59**, 1533 (1999).
- [16] D.F. Feder, C.W. Clark, and B. Schneider, Phys. Rev. A **61** (2000).
- [17] B. Jackson, J.F. McCann, and C.S. Adams, Phys. Rev. A **61** (2000).
- [18] T. Isoshima and K. Machida, Phys. Rev. A **59**, 2203 (1999).
- [19] S. Stringari, Phys. Rev. Lett. **82**, 4371 (1999).
- [20] P.O. Fedichev and G.V. Shlyapnikov, Phys. Rev. A **60**, R1779 (1999).
- [21] D.S. Hall, M.R. Matthews, J.R. Ensher, C.E. Wiemann, and E.A. Cornell, Phys. Rev. Lett. **81**, 1539 (1998).
- [22] J. Williams, R. Walser, J. Cooper, E.A. Cornell, and M. Holland, Phys. Rev. A **61** (2000); cond-mat/9904399.
- [23] J.J. Garcia-Ripoll and V.M. Pérez-Garcia, cond-mat/9910015.
- [24] S.-K. Yip, Phys. Rev. Lett. **83**, 4677 (1999).
- [25] T.-L. Ho, Phys. Rev. Lett. **81**, 742 (1998).
- [26] A.H. Carlsson, J.N. Malmberg, E.A. Ostrovskaya, T.J. Alexander, D. Anderson, M. Lisak, and Y.S. Kivshar, patt-sol/9909009.
- [27] D.S. Jin, J.R. Ensher, M.R. Matthews, C.E. Wieman, and E.A. Cornell, Phys. Rev. Lett. **77**, 420 (1996).
- [28] Y.S. Kivshar, J. Christou, V. Tikhonenko, B. Luther-Davies, and L.M. Pismen, Opt. Commun. **152**, 198 (1998).
- [29] *Hamiltonian Dynamical Systems*, Eds. R.S. MacKay and J.D. Meiss (Hilger, Bristol, 1987).
- [30] I. Aranson and V. Steinberg, Phys. Rev. B **53**, 75 (1996).

FIG. 1. Eigenfrequencies of the $|J| = 1$ perturbations of the unit vortex in state 1, $n = 1$. Dashed lines correspond to the numerical continuation of the frequencies given by Eq. (15). Symmetric set of negative eigenfrequencies is not plotted.

FIG. 2. Scenario of appearance of the drift instability of the unit vortex in the state 2, $n = 1$. (a) Frequencies of the resonant excitations for small values of g . Full lines – numerical results, dotted lines – asymptotic results, see Eq. (15). (b) Full lines – resonant eigenfrequencies ($Re\lambda$), dashed line – instability growth rate ($-Im\lambda$). Symmetric set of negative eigenfrequencies is not plotted.

FIG. 3. Scenario of appearance of the drift instability of the unit vortex in the state 2, $n = 9$. Full lines – resonant eigenfrequencies ($Re\lambda$), dashed line – instability growth rate ($-Im\lambda$). Symmetric set of negative eigenfrequencies is not plotted.

FIG. 4. The same as Fig. 5, but for $n = 0.3$.

FIG. 5. Growth rate of the drift instability of unit vortex in the state 2 vs n for different values of g . Full line: $g = 100$, dashed line: $g = 500$, dotted line: $g = 900$.

FIG. 6. Growth rate of the drift instability of unit vortex vs β_{12} , $g = 100$. Full line: $\beta_{22} = 0.97/1.03$; dashed line: $\beta_{22} = 1.03/0.97$

FIG. 7. Growth rate of the splitting instability of the double vortex in the state 1 vs g . Full line – $n = 10$, dashed line – $n = 20$.

FIG. 8. Growth rate of the drift $|J| = 1$ (full lines) and splitting $|J| = 2$ (dotted lines) instabilities of the double vortex in the state 2 vs n for different values of g . (a) $g = 100$, (b) $g = 900$.

FIG. 9. Development of the drift instability of the double vortex in the state 2: $g = 900$, $n = 2.5$. Top – $|\Psi_1|^2$, bottom – $|\Psi_2|^2$. Time interval between snapshots is 20. First snapshot corresponds to $t = 60$.

FIG. 10. Development of splitting instability of the double vortex in the state 2: $g = 900$, $n = 0.7$. Top – $|\Psi_1|^2$, bottom – $|\Psi_2|^2$. Time interval between snapshots is 20. First snapshot corresponds to $t = 30$.

FIG. 11. Evolution of the phases of the first (top) and second (bottom) condensate components, corresponding to the density profiles shown in Fig. 10. Color changing from black to white indicates the phase changing from $-\pi$ to π . Rough black lines indicate 2π phase jumps. Two unit vortices in the first condensate component are clearly seen in the third and fourth images of the top row.

FIG. 12. Phases of the unperturbed unit and double vortices. Color changing from black to white indicates the phase changing from $-\pi$ to π . Rough black lines indicate 2π phase jumps.

FIG. 13. Growth rates of the drift (full line) and splitting (dotted lines) instabilities of the double vortex vs β_{12} : $g = 100$, $\beta_{22} = 0.97/1.03$.

FIG. 14. Growth rate of the $|J| = 2$ splitting instability of the triple vortex in the state 1 vs g . Full line – $n = 1$, dashed line – $n = 0.2$.

FIG. 15. Growth rate of the shift $|J| = 1$ and splitting $|J| = 2, 3$ instabilities of the triple vortex in the state 2 vs n . (a) $g = 100$, (b) $g = 900$. Full lines - $|J| = 1$, dotted lines - $|J| = 2$, dashed lines - $|J| = 3$.

FIG. 16. $|J| = 2$ instability of the triple vortex in the state 2: $g = 900$, $n = 0.9$. Top - $|\Psi_1|^2$, bottom - $|\Psi_2|^2$. Time interval between snapshots is 15. First snapshot corresponds to $t = 70$.

FIG. 17. $|J| = 3$ instability of the triple vortex in the state 2: $g = 900$, $n = 0.9$. Top - $|\Psi_1|^2$, bottom - $|\Psi_2|^2$. Time interval between snapshots is 35. First snapshot corresponds to $t = 50$.

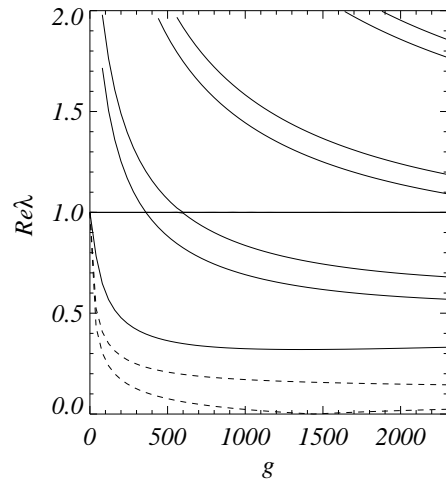


FIG. 1.

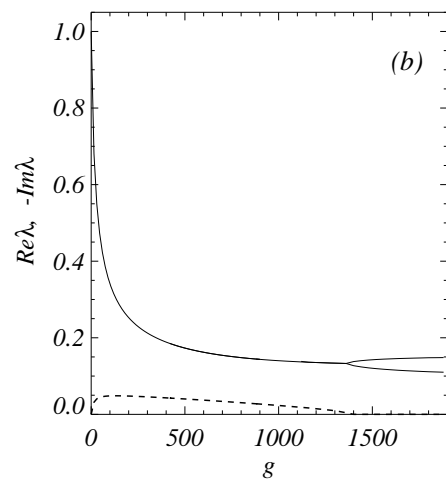
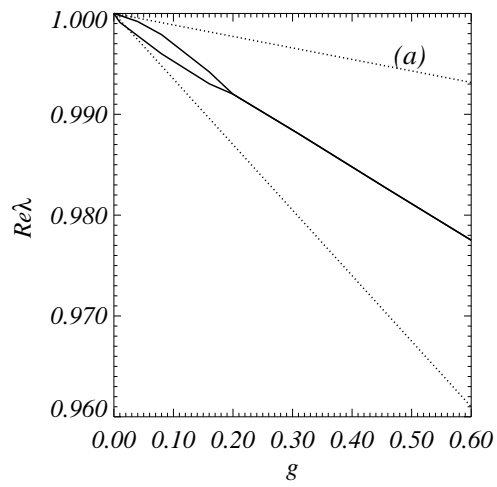


FIG. 2.

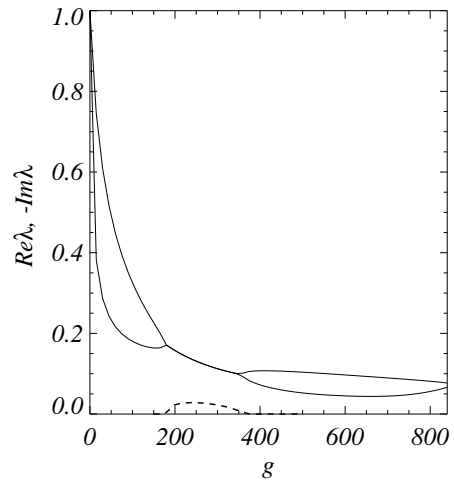


FIG. 3.

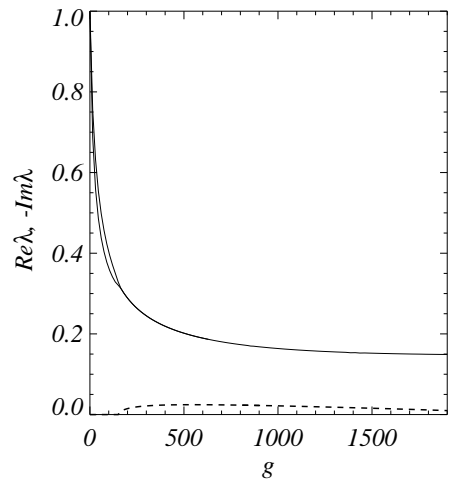


FIG. 4.

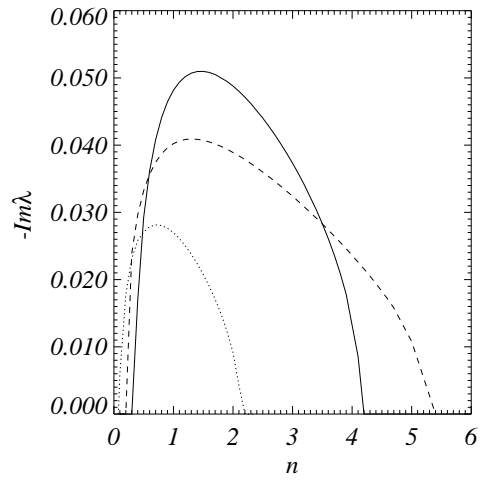


FIG. 5.

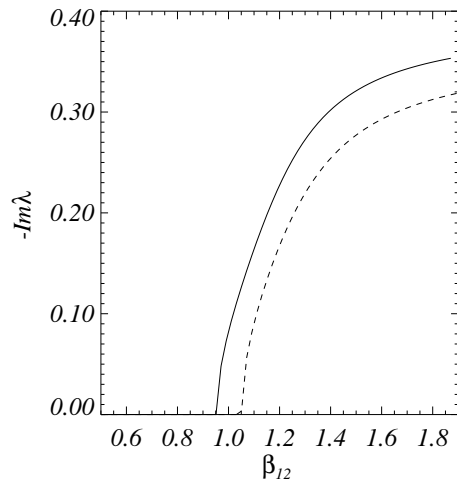


FIG. 6.

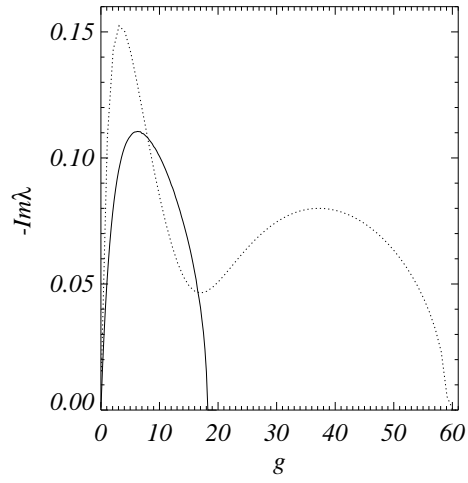


FIG. 7.

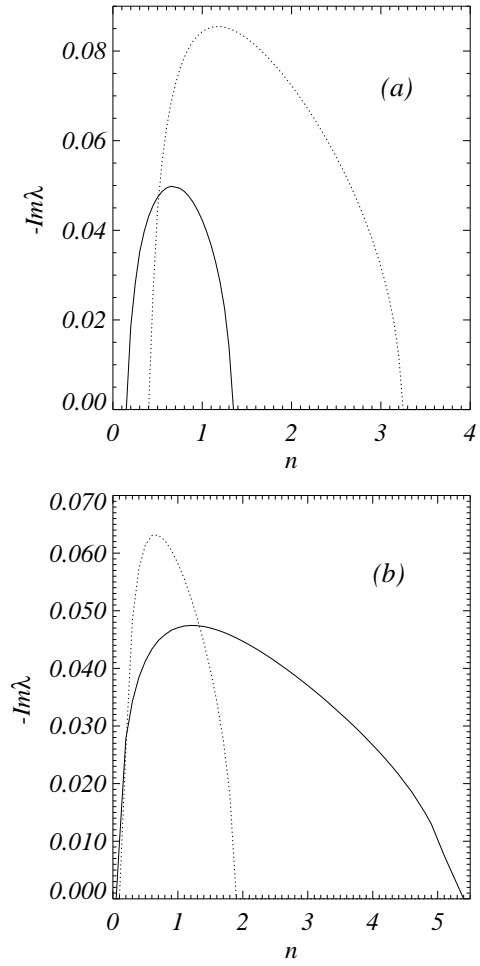


FIG. 8.

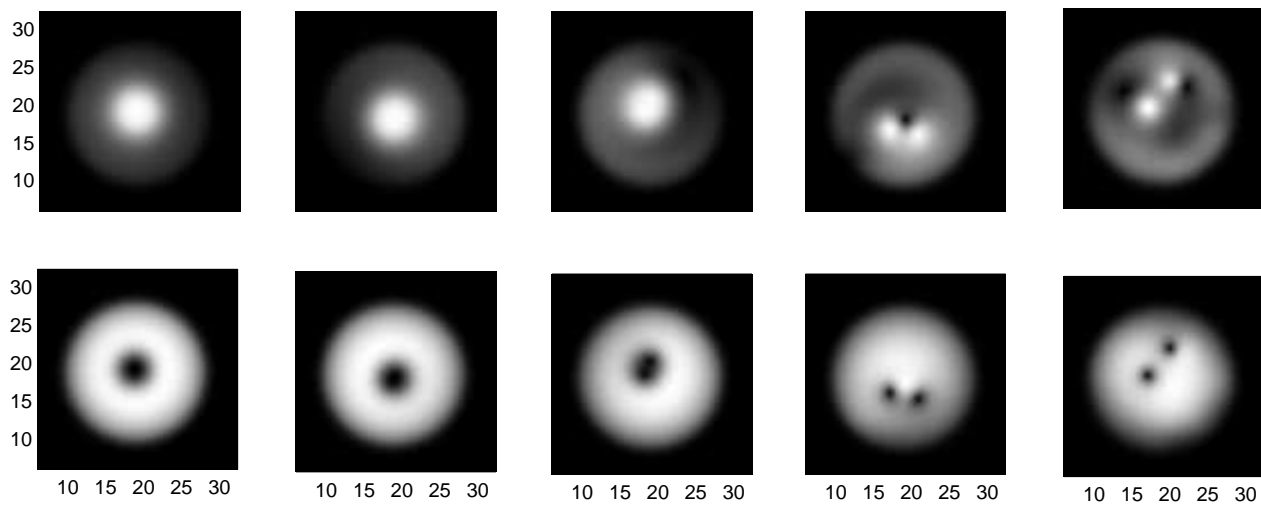


FIG. 9.

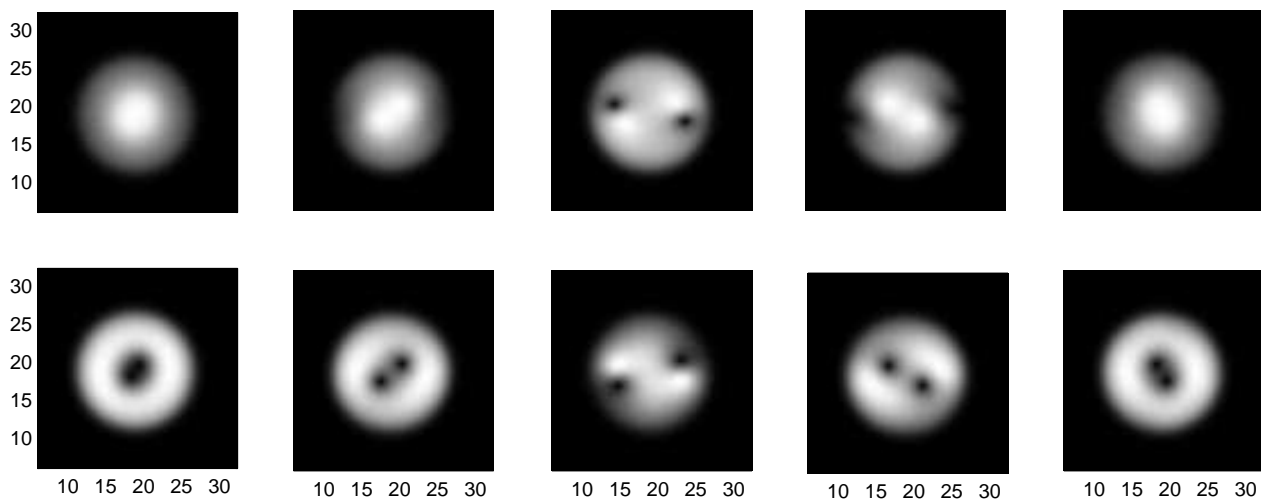


FIG. 10.

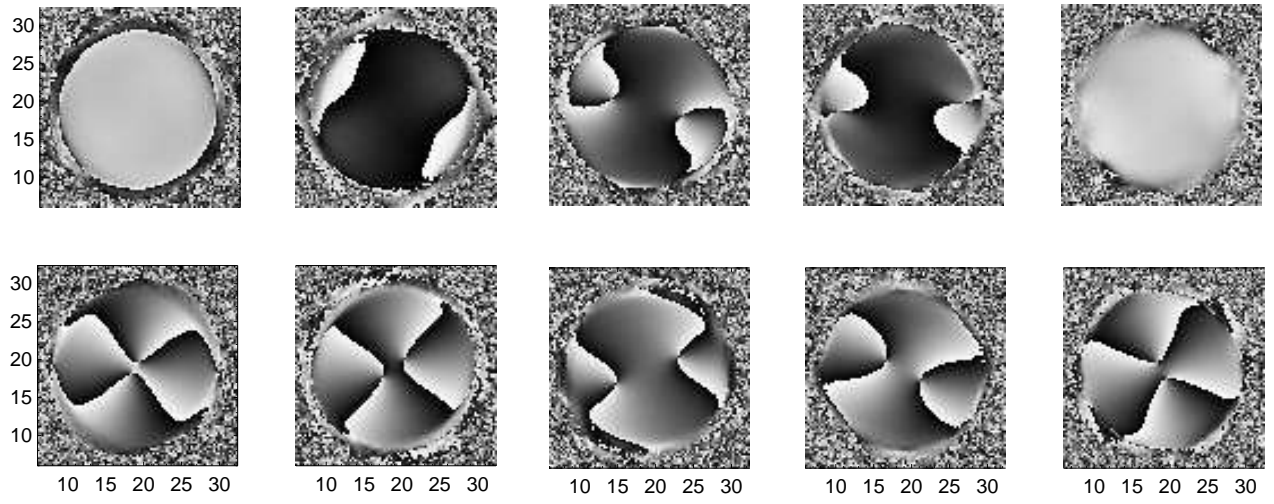


FIG. 11.

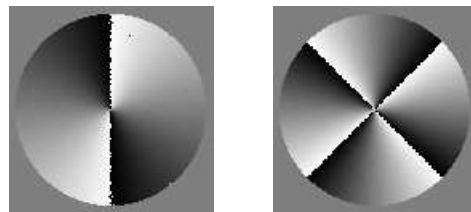


FIG. 12.

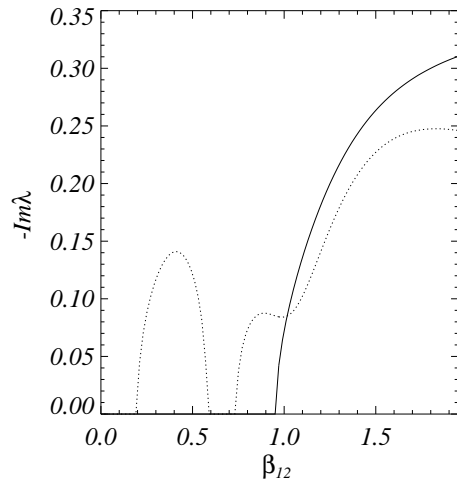


FIG. 13.

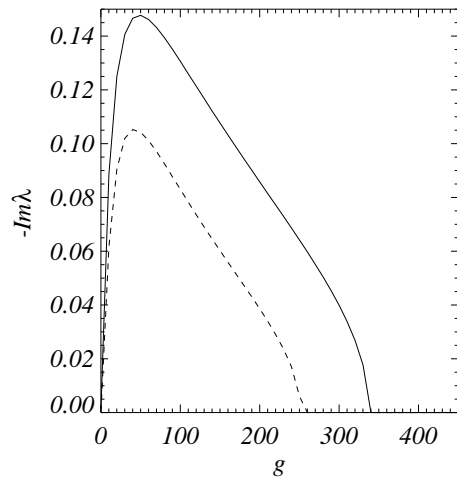


FIG. 14.

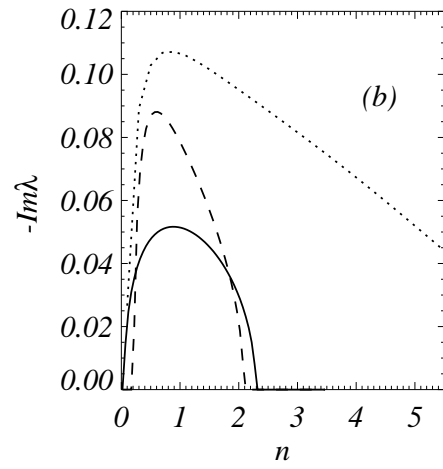
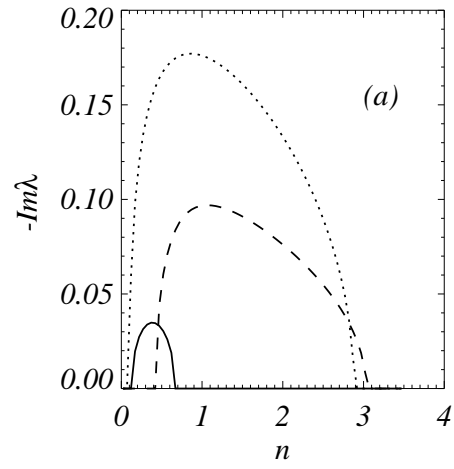


FIG. 15.

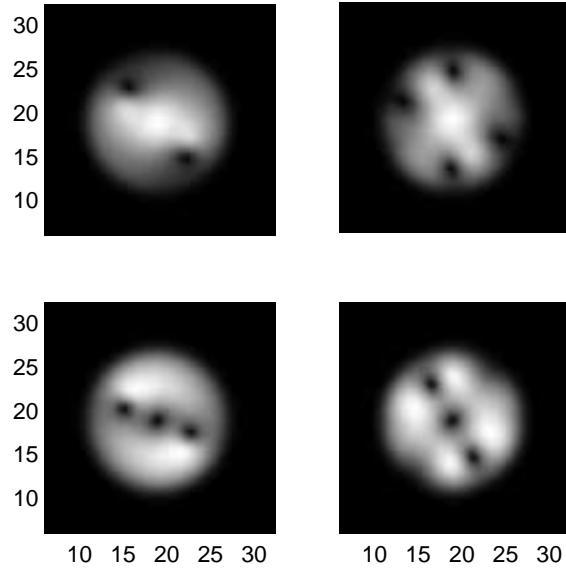


FIG. 16.

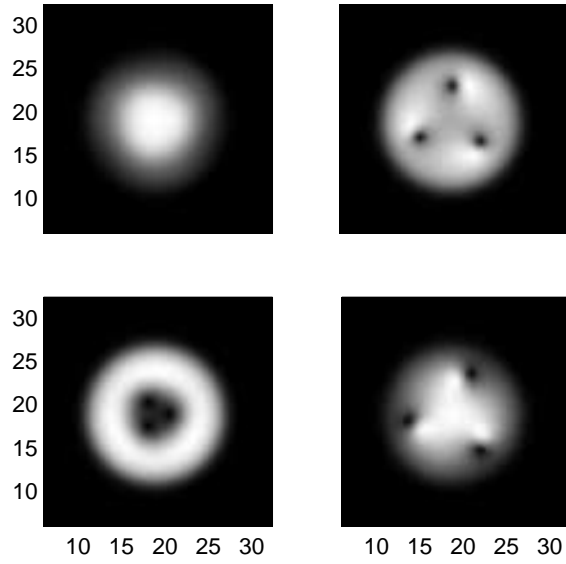


FIG. 17.